Journal of Hydrology: Regional Studies 61 (2025) 102745

Contents lists available at ScienceDirect

Journal of Hydrology: Regional Studies

journal homepage: www.elsevier.com/locate/ejrh

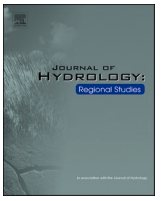

Integrating climate change and land use change into storm flood impact analysis in coastal cities

Qinke Sun [a,b,c], Johan Reyns [c,d,*], Jiayi Fang [e,**], Xiaoting Wang [c,f], Zhe Wang [g,h], Liang Zhou [a], Min Liu [b,**]

[a] Faculty of Geomatics, Lanzhou Jiaotong University, Lanzhou 730070, China
[b] Key Laboratory of Geographic Information Science (Ministry of Education), School of Geographic Sciences, East China Normal University, Shanghai 200241, China
[c] Department of Coastal and Urban Risk & Resilience, IHE Delft Institute for Water Education, Delft 2601DA, the Netherlands
[d] Deltares, Delft 2600 MH, the Netherlands
[e] Institute of Remote Sensing and Earth Sciences, Hangzhou Normal University, Hangzhou 311121, China
[f] History, Culture and Tourism School, Fuyang Normal University, Fuyang 311400, China
[g] Haihe River Water Conservancy Commission, the Ministry of Water Resources, Tianjin 300170, China
[h] State Key Laboratory of Hydraulic Engineering Intelligent Construction and Operation, Tianjin University, Tianjin 300072, China

ARTICLE INFO

Keywords:
Land use changes
Flood disasters
Climate change
SFINCS model
Coastal cities

ABSTRACT

Study region: Shanghai, China
Study focus: This paper proposes a comprehensive framework for quantifying storm surge floods in coastal cities by incorporating the influences of both climate change and urbanization. The framework achieves a physically process-based numerical simulation of storm surge-induced flood hazards due to tropical cyclones in coastal cities by coupling the fast flood inundation model (SFINCS) and the land use change model (GeoSOS-FLUS), along with the numerical nested model for storm surges (Delft 3D Flow & Wave). Using a 1000-year tropical cyclone simulated by the STORM model as an example, this study analyzes and maps coastal flood impacts under the moderate climate scenario (SSPs245) and high emission scenario (SSPs585), and also evaluates the impact of land use changes on these scenarios.
New hydrological insights for the region: Taking Shanghai, China as an example, the results show that by 2100, urban land use changes will lead to an increase in the extent of 1000-year TC flooding areas by 4.91–34.00 %, underestimating the inundation area of storm surges if future urban land use changes are not considered. Additionally, our predictions indicate the vulnerability of Chongming island and Changxing island to the impacts of climate change, despite the protective role of coastal embankments considered in the tropical cyclone storm surge simulation. The results of this study represent an important contribution to a better understanding of how future urban land use changes will affect storm surge flooding risks in and around Shanghai. The proposed methodology can be applied to coastal areas worldwide that are vulnerable to tropical cyclones, aiding in the formulation of hazard mitigation policies to alleviate flood impacts in these regions.

* Corresponding author at: Department of Coastal and Urban Risk & Resilience, IHE Delft Institute for Water Education, Delft 2601DA, the Netherlands
** Corresponding authors.
E-mail addresses: j.reyns@un-ihe.org (J. Reyns), jyfang@hznu.edu.cn (J. Fang), mliu@geo.ecnu.edu.cn (M. Liu).

https://doi.org/10.1016/j.ejrh.2025.102745
Received 17 May 2025; Received in revised form 14 August 2025; Accepted 25 August 2025
Available online 28 August 2025

1. Introduction

Floods are one of the most severe natural hazards worldwide (Hallegatte et al., 2013; Fang et al., 2020), in particular those resulting from storm surges occurring in coastal areas, and pose a significant threat to coastal development (Knutson et al., 2010). More than half of the world's population now lives within 100 km of the coastline (Sebastian, 2022), and coastal economies and communities face pronounced vulnerability to flood events (Hinkel et al., 2018; Koks et al., 2019). Flood events in coastal cities have caused huge property damage and loss of lives. For example, Hurricane Katrina storm surge breached the flood defenses in New Orleans, resulting in 218 deaths and over $96 billion in economic losses (Townsend, 2006). Hurricane Sandy caused flooding in coastal cities such as New York, resulting in 233 deaths and over $50 billion in economic losses (Diakakis et al., 2015). Typhoon Fitow affected over 7 million people in Zhejiang and Shanghai, causing enormous economic losses (Xu and Li, 2019). As coastal populations expand and urbanization accelerates under a changing climate, research consistently indicates that flood-related losses in coastal regions will escalate in severity (Ranasinghe et al., 2013; Vousdoukas et al., 2018; Mazumder et al., 2024).

Tropical cyclones (TC) are generally one of the major causes of coastal flooding events, as they usually cause the simultaneous occurrence of rainfall and storm surges (Orton et al., 2018; Gori et al., 2022). Assessing TC storm surge flood hazards requires a large amount of reliable TC information, especially for low-probability events (Bloemendaal et al., 2020). Due to the scarcity of TC event records, assessing TC storm surge flood events is more challenging. Researchers often employ statistical techniques to characterize potential tropical cyclone events within target regions by fitting probability models to historical distributions of essential storm attributes (e.g., central pressure and maximum wind radius) and drawing numerous synthetic samples from these fitted distributions. However, synthetic TC data relying on statistical methods are often limited to local data and cannot adequately consider future climate changes in TC (Bloemendaal et al., 2020; Dullaart et al., 2021). Research suggests that climate change will increase the impacts of TC events, with major TCs potentially showing more pronounced changes than lower category TCs (Bhatia et al., 2019). Therefore, to address the threats of flooding in coastal areas, it is essential to consider changes in storm surge floods generated by future changes in the TC climate, and quantify its impact on coastal areas.

In addition, urbanization is another important factor affecting coastal flood hazards (Zhang et al., 2018; Shao et al., 2020). Human-driven modifications to urban land use are widely recognized as a major factor in the future development of flood hazards (Jongman et al., 2014). Numerous studies have assessed how changes in land cover affect flood occurrence and risk (Adnan et al., 2020; Liu et al., 2023; Amare et al., 2024; Wu et al., 2024), showing that land use changes disrupts the hydrological balance—reducing surface infiltration, soil porosity, and water retention capacity—which can substantially alter runoff volumes (Schilling et al., 2010; Sajikumar and Remya, 2015; Guzha et al., 2018). Continued urbanization and varying development scenarios are therefore expected to exert differentiated influences on coastal flood hazards in the future.

However, most studies have either examined urban expansion's influence on tropical cyclone–induced storm surge flooding or assessed how climate change alters storm surge dynamics. Integrated analyses that evaluate the combined effects of climate change and urbanization on storm surge hazards are scarce. Some studies suggest the utility of integrating land use prediction models with hydrological/hydraulic models for quantifying flood hazard. For instance, Du et al. (2012) coupled the distributed hydrological model with land use prediction model to assess the impact of flood in Qinhuai River. Gori et al. (2019) combined land use models with

Fig. 1. Location of Shanghai, the red circular points are storm surge level verification stations, and the blue triangular points are astronomical tide verification stations.

hydrological modeling to estimate future floodplain extent in the Cypress Creek Wateershed. Pumo et al. (2017) developed a framework that links the physically based hydrological model tRIBS with a cellular automata (CA) model to assess hydrological change in the Eldon River Basin. Similarly, Sun et al. (2022) proposed combining flood inundation and urban expansion to assess the impact of future flood hazards, but this method ignores the effects of land use changes on flood inundation. At the same time, these methods have been applied less in the framework of assessing storm surge flood hazards in coastal areas. Previous studies have concentrated on the effects of climate change and urban growth on watershed floods, without considering how these changes might influence storm surge flood hazards in coastal areas.

This study presents a comprehensive framework to quantify future storm surge flood hazards in coastal areas by considering the combined effects of climate change and urbanization. The framework relies on storm surge hydrodynamic models, land use prediction models, and a flood inundation model. Specifically, we establish an urban flood coupled model based on the Super-Fast INundation of CoastS (SFINCS, Leijnse et al., 2021) model and the Future land use simulation model (GeoSOS-FLUS, Liu et al., 2017). This coupled model is integrated with the storm surge numerical nested model (Delft3D, Lesser et al., 2004) to simulate storm surge flood hazards caused by TC in coastal cities. The Delft3D model uses TC tracks simulated by the Synthetic Tropical cyclOne geneRation Model (STORM, Bloemendaal et al., 2020) algorithm based on climate model outputs as forcings to simulate storm surge water levels. The FLUS model uses future climate scenarios to develop changes in land use for study areas. By chaining these components, our approach enables quantification of changes in TC surge hazards across multiple future climates scenarios and evaluation of how land-use alterations modify estimated flood extents. We demonstrate the framework in the estuarine coastal region of Shanghai, China—a rapidly

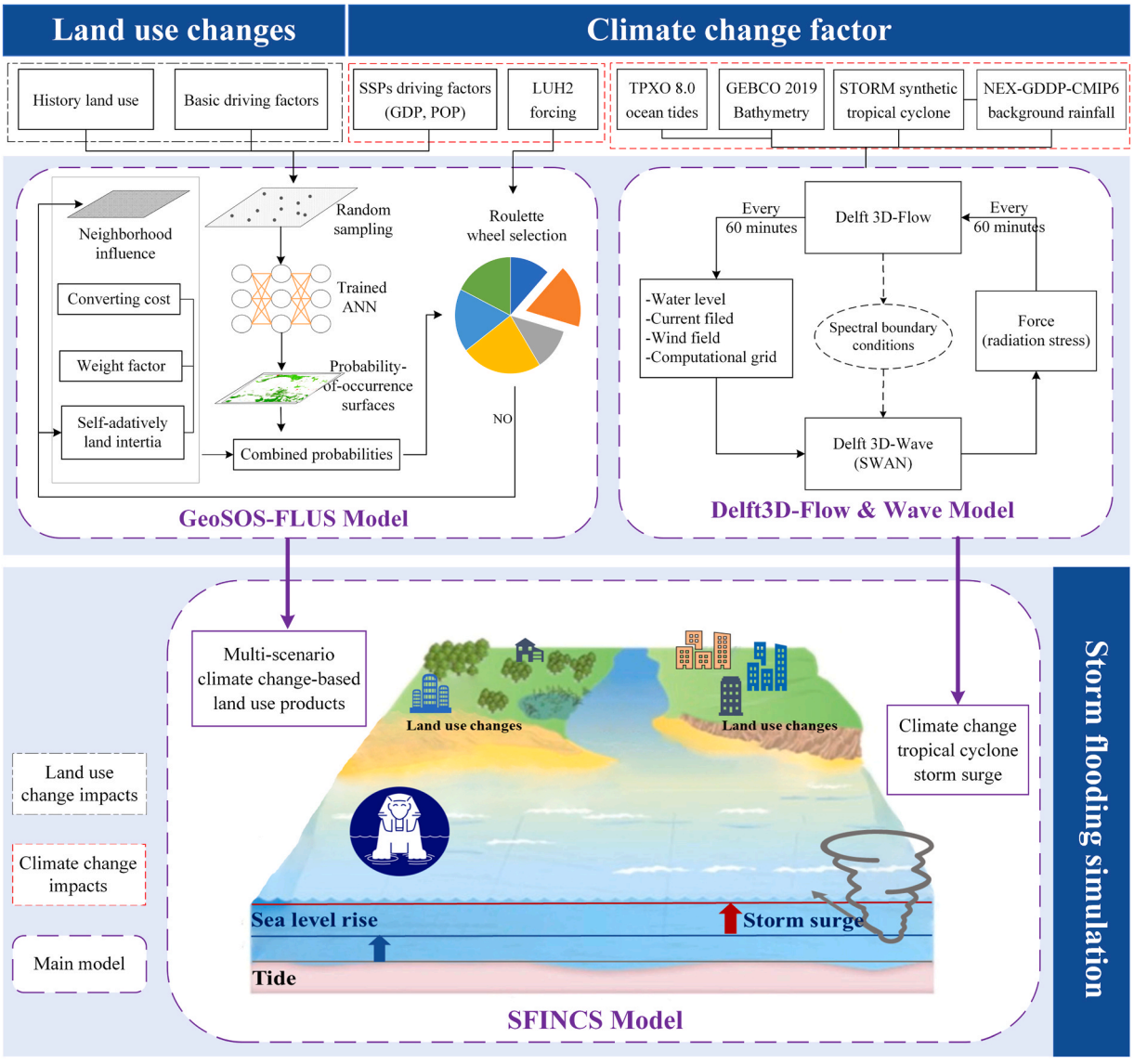

Fig. 2. The overall flow chart of research.

urbanizing area with pronounced vulnerability to cyclone-induced storm surges.

2. Study area

Shanghai is situated in China's Yangtze River Delta and covering 0.06 % of the national landmass. The municipality includes the alluvial islands of Chongming, Changxing and Hengsha (Fig. 1), which have formed at the river's estuary through sediment deposition. Spanning roughly 120 km by 100 km, its average elevation is only about 4 m above mean sea level. This predominantly flat, low-lying terrain offers minimal natural defense against storm surges, rendering Shanghai especially vulnerable to coastal flooding (Du et al., 2020). Indeed, global assessments have identified Shanghai as one of the most flood-vulnerable urban centers (Hallegatte et al., 2013) and among the top ten cities worldwide in terms of population and asset exposure to coastal inundation under future climate scenarios (Hanson et al., 2011). Historical records indicate that Shanghai experiences tropical cyclone–induced storm surges two to three times annually (Zong and Chen, 2002). As a major national and international financial hub, Shanghai's dense socio-economic concentrations heighten its sensitivity to flood hazards exacerbated by global climate change.

3. Materials and methods

3.1. Methodological approach overview

The methodology presented in this paper links land use projection modeling and storm surge hydrodynamic modeling to more accurate understanding of the potential impacts of a range of future development scenarios on coastal flooding caused by TC. The methodology consists of three main components: (1) GeoSOS-FLUS modeling to simulate future land use changes under SSPs245 moderate and SSPs585 high emission climate scenarios; (2) Delft3D modeling to simulate storm tides and surges from a 1000-year TC event; and (3) SFINCS modeling to map coastal flood hazards and assess the potential impacts of land use changes on flooding (Fig. 2). GeoSOS-FLUS calibration and validation are based on high-quality historical land use/land cover (LULC) maps derived from Landsat imagery for 2010, 2015, and 2020, selected to capture significant urbanization phases in Shanghai and provide adequate spatial resolution. The storm tides and surge hydrographs generated in the Delft3D model were fed to the Super-fast coastal inundation model to derive maximum water levels and flood depths. These results support impact assessment of land use changes on future coastal flood hazards.

3.2. Delft3D Flow & Wave model

Delft3D is a powerful and flexible hydrodynamic simulation program developed by Deltares (Lesser et al., 2004). It consists of several models that can interact with each other including Delft3D Flow, Delft3D Wave and others. These models can be used for the simulation of changes in processes such as water flow, wave, and water quality in time and space respectively. We simulate storm surge

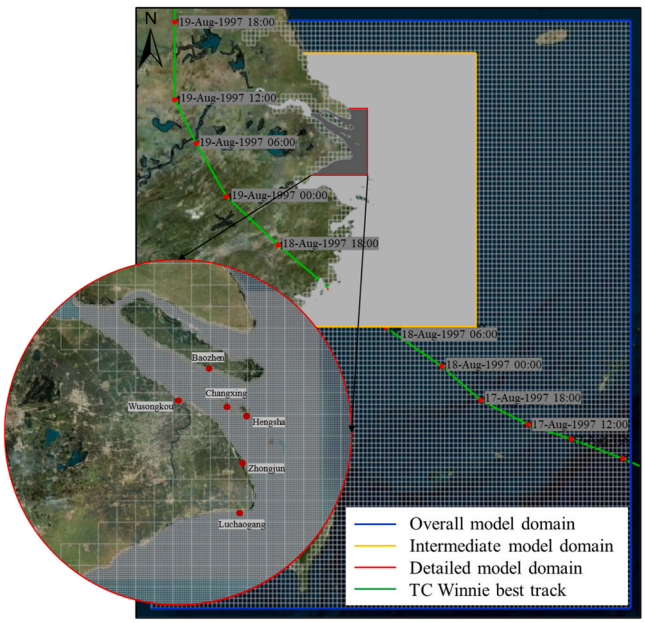

Fig. 3. Model chain with 3 model domains for simulation of flooding due to TC Winnie. (The overall model domain and intermediate model domain are the Delft3D-Flow & wave models, and the detailed model domain is the SFINCS model. The large model is shown in blue; the intermediate model is shown in yellow; the detailed model is shown in red, and the best track of TC Winnie is shown in green.).

waves by modelling the interaction between Delft3D Flow and Delft3D Wave. This coupled model can effectively simulate the spatial and temporal change of storm water levels due to TC and has been successfully applied to many coastal and estuarine areas (Bastidas et al., 2015; Lyddon et al., 2019). In this study, Delft3D Flow & Delft3D Wave is used to hindcast the hydrodynamic response of the Shanghai area to TC Winnie (Wang et al., 2018). This TC originated from a tropical disturbance in the western Pacific on 8 August 1997. After formation, it tracked steadily northwestward while intensifying, making landfall on the evening of 18 August with a central pressure of approximately 960 hPa and peak surface winds near 40 m/s. Its passage produced Beaufort 8–10 gales over Shanghai, rainfall totals exceeding 50 mm (with localized peaks above 150 mm), and drove tidal levels in both the Yangtze River Estuary and the Huangpu River beyond their historic maxima.

3.2.1. (1) Delft 3D Flow & Wave model setup

A three-step nested modeling chain was established (Fig. 3) to simulate cyclone-driven storm tides and surges in near-coastal zones. The outermost Delft3D Flow & Wave model domain spans the regional scale with a 0.1° grid, forced by tidal constituents (amplitude and phase) from Oregon State University (OSU) Tidal Inversion Software (OTIS), background meteorological inputs (e.g., rainfall fields from NEX-GDDP-CMIP6), and parametric wind and pressure fields derived from China Meteorological Administration (CMA) best-track data (Lu et al., 2021) using the Holland profile (Holland et al., 2010) and formatted into a spiderweb grid (Deltares, 2021). Open boundary conditions for water level and waves were defined along the eastern edge of the domain in open ocean areas (blue border in Fig. 3). An intermediate Delft3D domain at 0.01° resolution inherited time-varying water levels and wave spectra along its boundaries from the outer model (yellow border in Fig. 3). This domain was designed to better resolve hydrodynamic processes near the Shanghai coastal zone.

Finally, the high-resolution (100 m) SFINCS model was nested within the intermediate model. It received boundary conditions in the form of storm surge water level and wave-induced setup, provided along an open coastal boundary located 2–5 km seaward of the Shanghai shoreline. The position of this boundary was selected based on bathymetric contours and model stability and is indicated in red border in Fig. 3. The setup of the SFINCS model is detailed in Section 3.4.

For the nested models, the basic data of the General Bathymetric Chart of the Oceans (GEBCO_2022) offshore depths and Shuttle Radar Topography Mission (SRTM) nearshore elevations are used. 111 × 121 grid cells form the large model and 580 × 567 grid cells form the intermediate model. The wind drag coefficient was used as proposed and validated by Chu et al. (2019) in the East China Sea region. We calibrated and validated the model by simulating with and without TC storm surge.

The tidal validation data are taken from the IHO (International Hydrographic Observatory, IHO), and TC Winnie storm tides data are from the Shanghai Climate Centre of Shanghai Meteorological Bureau and referenced to the study by Yin (Yin, 2020), and the location information of the observation stations is shown in Fig. 1.

Reliable and extensive TC track data is required to evaluate the storm surge disasters caused by TC. However, assessing the risks associated with tropical cyclones is challenging due to the relatively scarce data on their occurrence. To account for climate change impacts on tropical cyclone activity, we used the STORM synthetic TC dataset, which integrates climate perturbations from four high-resolution GCMs: CMCC-CM2-VHR4, CNRM-CM6–1-HR, EC-Earth3P-HR, and HadGEM3-GC31-HM (Bloemendaal et al., 2020). These models were selected in the original STORM framework for their ability to simulate realistic cyclone characteristics and for their participation in the HighResMIP initiative under CMIP6. In this study, we used synthetic TC tracks derived from the EC-Earth3P-HR model under the SSP5–8.5 scenario, which reflects a high-emission future. This model was chosen as it represents one of the more extreme projections in terms of cyclone intensity and frequency, providing a conservative assessment of future coastal flood hazards.

The 1000-year return period was chosen to analyse extreme, low-probability events, which are essential for understanding the potential storm surge hazards under future climate scenarios. Specifically, this approach ensures the simulated storm surges encompass the magnitude of extreme events such as those caused by TC Winnie (100-years), providing valuable insights into future scenarios.

3.2.2. (2) Delft 3D Flow & Wave model validation

We validate the model's performance by simulating two events: astronomical tide and tide with storm surge, and assess the consistency and accuracy of the model using three evaluation metrics, namely Nash-Sutcliffe Efficiency (NSE), Root Mean Square Error (RMSE) and Bias. Table 1 summarizes the NSE and RMSE statistics. During non–tropical cyclone periods, simulated astronomical tides were compared to measurements from Shanghai–area tidal gauges Fig. 4, with an average RMSE of 0.18 m, a mean bias of 0.02 m, and an NSE of 96.80 %, indicating good performance of tide prediction. Comparing the simulations with the observations during the period of TC Winnie (Fig. 5), simulated surge-augmented tides closely matched observed phase and timing, indicating the model effectively reproduces dominant tidal constituents and surge dynamics. Across these stations, surge performance metrics averaged an RMSE of

Table 1
Error of model validation for water level during TC Winnie and tides.

Tide Validation	Luhuashan	Westvolcano	Shaweishan	Tungsha	Average
NSE (%)	96.27	97.77	98.34	94.85	96.80
RMSE (m)	0.22	0.16	0.14	0.20	0.18
Bias (m)	−0.07	0.02	0.05	0.08	0.02
TC Validation	Luchaogang	Xiaoyangshan	Changxing	Wusongkou	Average
NSE (%)	95.14	96.67	94.02	92.42	95.06
RMSE (m)	0.32	0.25	0.32	0.30	0.30
Bias (m)	0.09	0.02	0.10	0.09	0.08

0.33 m, NSE of 94.17 %, and bias of 0.08 m, reflecting robust storm surge simulation skill. Although the simulation results show an underestimation before and after the storm peak at some tidal stations, this phenomenon may be due to the model does not fully accounting for the effects of bathymetric and bed roughness at that time. Overall, the model simulates both tidal and storm surges tide with high NSE values and low RMSE values, confirming the good simulation performance of the model.\

3.3. GeoSOS-FLUS model

The GeoSOS-FLUS model is the land use change simulation model based on the Geosimulation and Optimization System (GeoSOS, Li et al., 2011; Liu et al., 2017). Unlike earlier CA formulations (Logistic-CA, Chen et al., 2014、CLUE-S, Verburg et al., 2002), GeoSOS-FLUS combines a top-down system dynamics module with a bottom-up CA mechanism to address complex spatial dynamics. Additionally, it integrates an artificial neural network (ANN) model to address the complex nonlinear relationship between historical land use and data of various influencing factors. The Simulation proceeds in two stages: 1) using ANN to train and estimate the probability-of-occurrence of different land use types on the cells within the study area, 2) using CA with adaptive inertia and competitive mechanisms to simulate interconversions between different land use types. Then the simulation and prediction of complex land changes under specific scenarios are accomplished.

3.3.1. (1) GeoSOS-FLUS model setup

The ANN model has been proven to be an effective method for solving various nonlinear geographic problems (Li and Yeh, 2002; Qiang and Lam, 2015). The ANN training leverages twelve spatial predictor layers, including historical and current land use types, traffic networks (highways, railways, subways, main roads et), natural conditions (elevation, slope), socio-economic and locational data (POP, GDP, and city centres), and future climate change product data (Table 2). All rasters were regridded to a uniform 100 × 100 m resolution and a normalization function was used to cast all data in the range of [0, 1]. The resampling involved both upscaling (e.g., for socio-economic and climate data originally at 1 km or coarser resolutions) and downscaling (e.g., for DEM and slope data at 30 m resolution), depending on the original resolution. The resampling method was selected based on data type, for categorical variables, the nearest neighbor method was used to preserve discrete class boundaries and avoid misclassification during

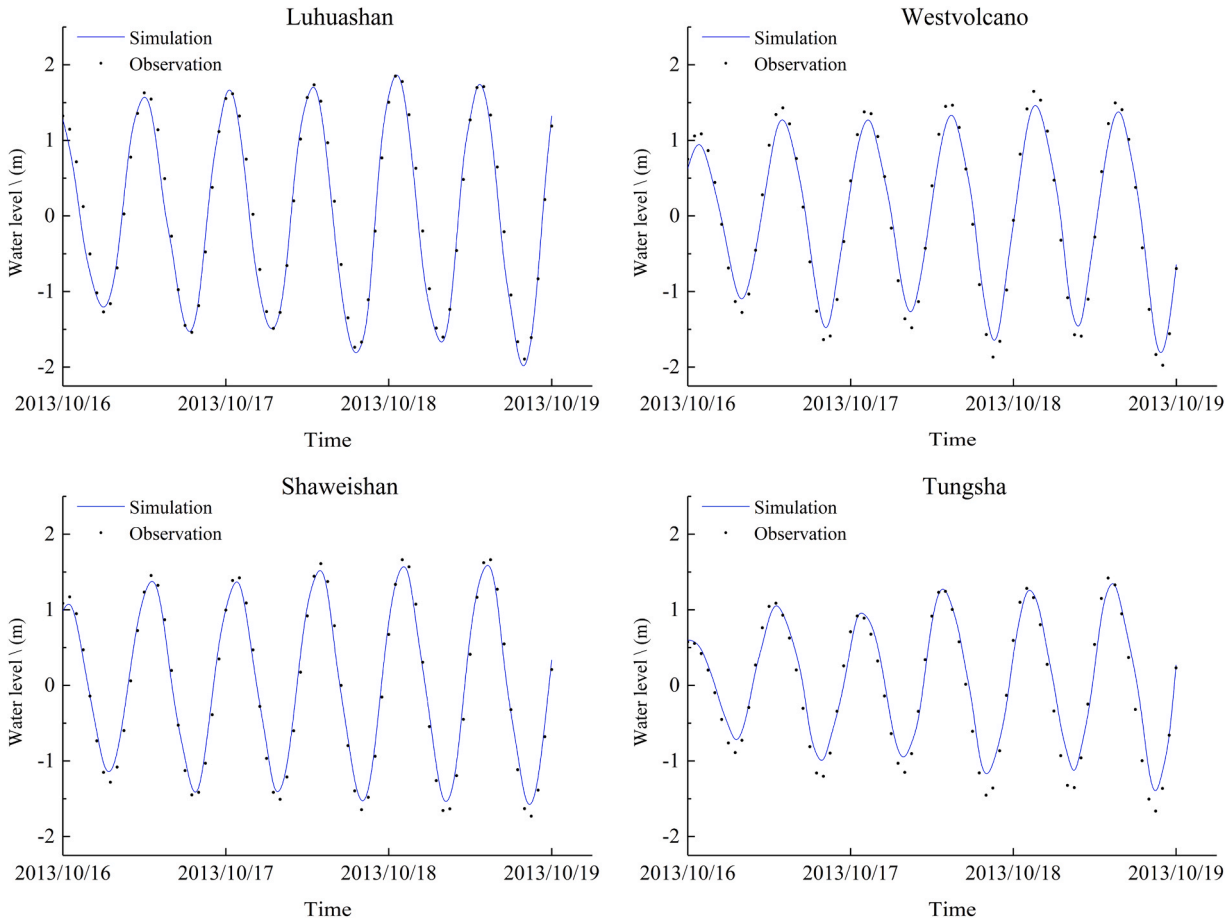

Fig. 4. Comparison between tidal simulation results and measured values. The location of the stations is indicated in Fig. 1.

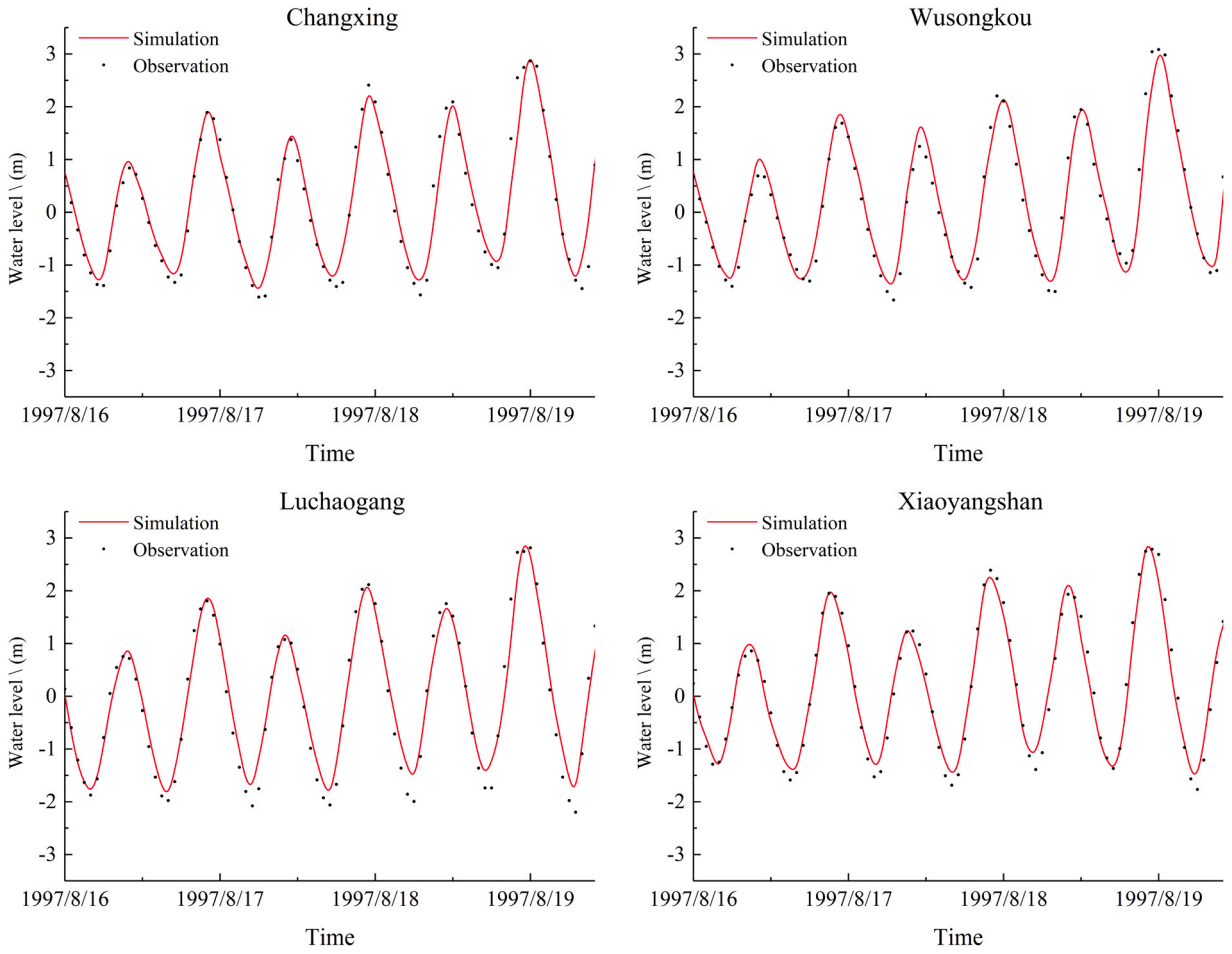

Fig. 5. Comparison between storm surge simulation results and observed values. The location of the stations is indicated in Fig. 1.

Table2
Driving factors in GeoSOS-FLUS model.

Data Category	Data Class	Resolution	Resampling Direction	Data Type	Data Source
Land use	2010–2020 land use	100 m	-	Categorical	Resource and Environmental Data Cloud Platform (http://www.resdc.cn)
Traffic network	Highway Railway Subway Main roads	Vector	Vector to Raster (100 m)	Categorical	OpenStreetMap (https://www.openstreetmap.org)
	Airports Train stations				Tencent Map (https://map.qq.com/)
Location factors	City center	Vector	Vector to Raster (100 m)	Categorical	Tencent Map (https://map.qq.com/)
Natural factors	DEM Slope	30 m	Downscaling	Continuous	ASTER GDEM (https://earthexplorer.usgs.gov/)
Social economy	GDP Population	1 km	Upscaling	Continuous	Resource and Environmental Data Cloud Platform (http://www.resdc.cn)
Climate change predictions	GDP projection under SSPs	30″	Upscaling	Continuous	Scientific data (https://www.nature.com/articles/s41597-022-01300-x)
	Population projection under SSPs	30″	Upscaling	Continuous	Scientific data (https://www.nature.com/articles/s41597-020-0421-y)
	LUH2	0.25°	Upscaling	Continuous	University of Maryland (https://luh.umd.edu/)

Note: LUH2 is the abbreviation of Land-Use Harmonization 2.

interpolation. For continuous variables, bilinear interpolation was applied to maintain spatial gradients and smooth transitions. Accuracy was evaluated using 20 % random samples. For continuous data, RMSE remained within 5 % of the value range. For categorical data, Kappa coefficients between original and resampled land use rasters ranged from 0.87 to 0.89. These results confirm minimal information loss and justify the resampling strategy. Further details are provided in Supplementary Table S1.

The ANN model was designed with 12 neurons in the input layer (corresponding to the 12 spatial drivers), and 5 neurons in the output layer (corresponding to the 5 land use types). We used land use/land cover (LULC) maps from 2010 and 2015 as training inputs for the ANN model, and validated the model using the observed land use in 2020. The training results of the ANN algorithm were evaluated using the RMSE, and the sampling training was stopped when the RMSE was less than 0.20 (Liu et al., 2017). Here, we first use the current spatial variables to train the ANN model and then consider future climate change scenarios by replacing the current spatial variables with future climate change spatial variables. Analysis of the ANN-derived predictor weights enabled quantification of each spatial variable's influence on land-use allocation. Fig. 6 shows that POP, GDP, and distance from subways and airports are important influences on urban land use change.

After calibrating the ANN and producing probability-of-occurrence maps, the CA simulation phase is executed, wherein each cell's transition is determined by its occurrence probabilities in conjunction with neighborhood effects, conversion costs, and a roulette wheel selection. In order to maximize the conversion probabilities for each cell, we set the neighborhood size to 3, meaning that the CA adopts a 3×3 cell neighborhood condition. The conversion costs represent the ease or difficulty of a cell change from one land use type to another. The values of conversion costs range between 0 and 1, with a value of 1 signifying almost impossible conversion. We used conversion costs provided by previous land use simulations in Shanghai (Sun et al., 2022). Finally, the conversion status of the cells was determined by combining the values generated based on roulette wheel. The selection of values for the roulette wheel is randomly generated, and it is precisely because of this randomness that the CA can better reflect the uncertainty in the dynamics of real-world LULC.

Finally, the amount of future land use type demand uses the projected amount of LULC for the target year under the Land-Use Harmonization 2 (LUH2) climate change scenario. Meanwhile, we adjust the future amount of LULC for the study area to match the simulation requirements using the data processing methods proposed by Hou et al. (Hou et al., 2022). We selected two climate scenarios for simulations-SSPs245 and SSPs585-which represent a range of development possibilities under the influence of future climate trends and land use policies.

3.3.2. (2) GeoSOS-FLUS model validation

We assessed GeoSOS-FLUS by projecting 2020 land-use patterns from 2015 baseline data. The simulated map exhibited strong spatial concordance with the observed 2020 distribution (Fig. 7). The land use maps were obtained from the China's National Land Use and Cover Change (CNLUCC) dataset, which has been extensively validated. The overall agreement (OA) of land use classification exceeds 94.30 %, and the polygon identification accuracy reaches 98.70 % (Xu et al., 2018), ensuring the reliability of the training and validation data used for simulation. Furthermore, we measured the model's output accuracy to validate its precision. By comparing the simulated results with the actual results on a per-pixel basis and calculating the confusion matrix, we found an OA of 93.20 % and the Kappa coefficient (Kappa) of 0.8942. These results confirm the model's suitability for spatial simulation and forecasting of land use change in Shanghai.

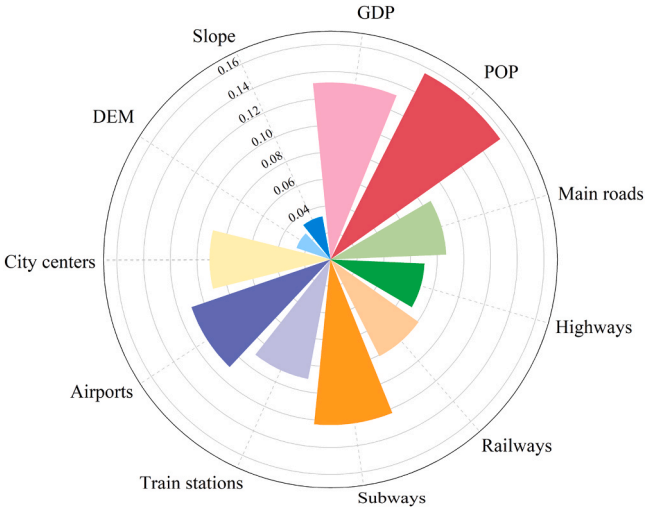

Fig. 6. Spatial variable importance measures based on ANN model.

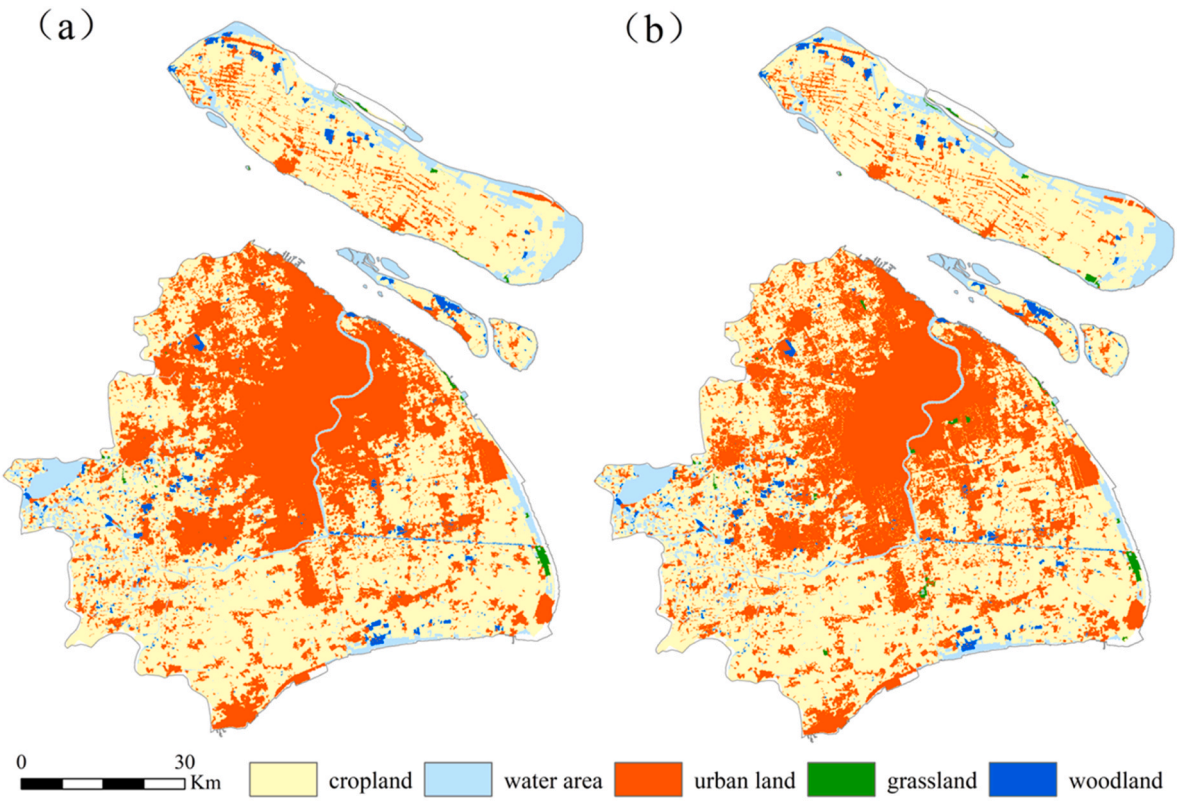

Simulated Type	Crop land	Water area	Urban land	Grass land	Wood land	Actual Type	Crop land	Water area	Urban land	Grass land	Wood land
Area (km^2)	3625.54	481.85	2439.13	23.75	106.27	Area (km^2)	3756.92	481.85	2309.36	26.74	101.67

Fig. 7. Comparison of simulated (a) and actual (b) land use types in Shanghai in 2020.

3.4. SFINCS compound flood model

SFINCS is a novel and highly efficient compound flood model. It was selected for its capacity to rapidly simulate multi-process flooding dynamics with low computational demands while achieving accuracy on par with single-driver approaches such as Delft3D (Leijnse et al., 2021). SFINCS employs two-dimensional Local Inertial Equations (LIE) for its continuity and momentum formulations (Bates et al., 2010). In this scheme, using a temporal increment (Δt) of 60 s and spatial grid sizes (Δi) of 100 m in the x and y directions are discretized to calculate volumetric flow per unit width at the subsequent timestep ($t + \Delta t$), after which water levels are updated using the continuity equation. The continuity equation of the SFINCS model also incorporate the gridded rainfall and discharge as local source terms. In addition, compared to the original LIE formulation, the SFINCS momentum equation includes two additional terms: the wind drag term $\tau_{w,x}$ and the advection term adv_x, which simulate the locally generated wind set-up and wave runup, respectively. They receive input from other sources or models to simulate wave run-up in coastal areas. This is also the reason why SFINCS is combined with tools for simulating wind and wave effects.

$$r_i^{t+\Delta t} = \frac{r_i^t - (g d_i^t \frac{\Delta z}{\Delta i} + adv_i - \frac{\tau_{w,i}}{p_w})\Delta t}{1 + \frac{g \Delta t n^2 r_i^t}{d_i^{t\,7/3}}} \tag{1}$$

Where r_i^t is the flow rate at time t. d_i^t indicates the average water depth between two adjacent grids. Δi is the grid size, Δz is the water level difference between these grids, and p_w is the water density. g and n indicate the gravitational constant and the Manning friction coefficient, respectively. As mentioned above, $\tau_{w,i}$ is to simulate of locally generated wind set-up, and adv_i is used to account for the long wave runup.

3.4.1. (1) SFINCS model setup

The setup of the SFINCS model includes the model domain and the mask domain. The model domain of SFINCS is divided into rectangular grids based on the coverage of the study area, with a grid cell resolution of 100 × 100, and the model domain yields a total of 1300 × 1560 grid cells. The mask domain is also the range of the active grid, we set the active grid to start from the −2 m contour on the seaward side of the domain, and combine it with the administrative boundary of Shanghai. In this model, SFINCS solves 677,143 active cells, which account for 33 % of the total grid cell count. Boundary conditions for storm surge water levels and wave action are supplied by the nested Delft3D Flow & Wave model. Moreover, besides using the same bathymetry, the SFINCS model also uses SRTM topographic data including coastal embankment elevations, to improve the accuracy of the flood inundation mapping. The coastal embankment data comes from the Shanghai Water Authority (https://swj.sh.gov.cn/). Furthermore, SFINCS model also add LULC information to simulate the potential impact of land use changes on flooding.

Land cover data representing Winnie conditions in the study area were obtained at 30 m resolution from the 1995 dataset (Xu et al., 2018). In SFINCS model, each land cover class is parameterized through a cell-specific Manning's roughness coefficient, which affects the rate of overland flood spreading (Kalyanapu et al., 2009). Therefore, areas covered with vegetation will have a higher friction coefficient and lower flow rates, while urban areas and impervious areas will have lower friction coefficients and higher flow rates. Based on previous studies (Sun et al., 2022), land cover types were converted to spatially varying Manning's coefficients, assigning values of 0.23, 0.85, 0.22, and 0.14 to cropland, woodland, grassland, and urban land, respectively. The future land cover simulated by the GeoS0S-FLUS model was converted into spatially varying Manning's coefficients for SFINCS prediction analysis. In addition, sea-level rise projections under SSPs245 and SSPs585 were added to the tropical cyclone–induced surge heights, enabling the evaluation of the impact of storm surge flooding under different future climate scenarios.

3.4.2. (2) SFINCS model validation

We compared the peaks water surface elevations simulated by SFINCS for multiple time periods before and after the real storm surge with the high water marks (HWM) recorded at the coastal observation station during the same period to validate the model's performance in simulating the highest water levels. Fig. 8 shows the comparison between the simulated peak water surface elevations and the HWM at the observation station. The observation station record data was obtained from Pan et al. (Pan and Liu, 2019). The simulation results indicate a relatively good agreement between the simulated peak water surface elevations and the observed HWM data, as well as a high degree of consistency between the timing of maximum peaks at each station and the HWM records. Although the model slightly underestimates the water levels at some observation stations, it produces good results in predicting extreme storm surge water levels. Therefore, the simulation results of HWM indicate that the simulation performance of the SFINCS model is suitable for flood inundation simulation.

4. Results

4.1. Future land use changes

We set two different climate change scenarios and predicted land use changes in Shanghai in 2100. The year 2100 was selected to represent a far-future high-emission scenario, capturing the cumulative impacts of climate change and land use expansion over the century. This time horizon aligns with the SSP/CMIP6 frameworks and allows the assessment of long-term risk trajectories under worst-case conditions. While near-term projections (e.g., 2050) are important for decision-making, the 2100 scenario provides an essential reference for long-range infrastructure planning and climate resilience stress-testing. The land use simulation results indicate that urban expansion will predominantly occur along the periphery of the existing built-up area, effectively enlarging the current urban footprint. As shown in Fig. 9, the projections also show different development patterns under the two different scenarios. Under

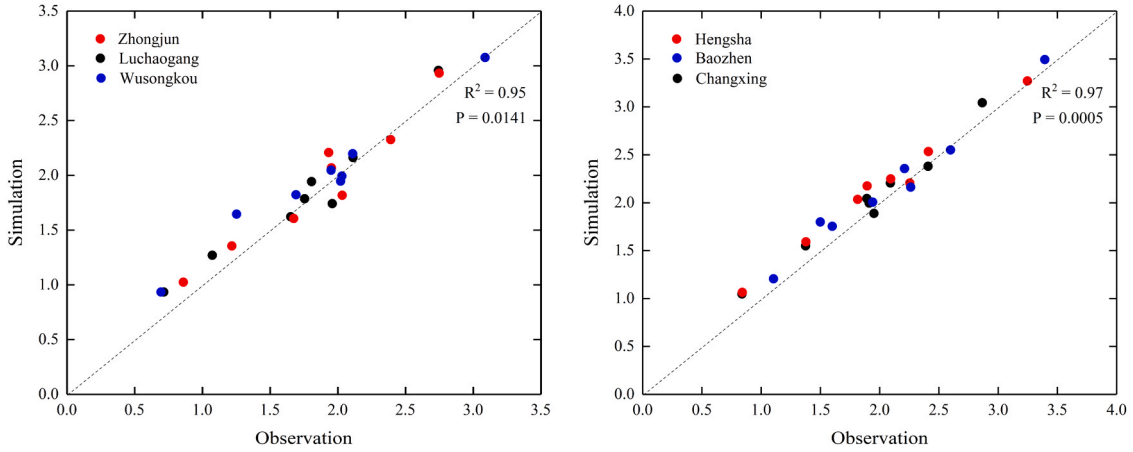

Fig. 8. SFINCS performance on HWM at the six different observation gauges. (Vertical datum is mean sea level).

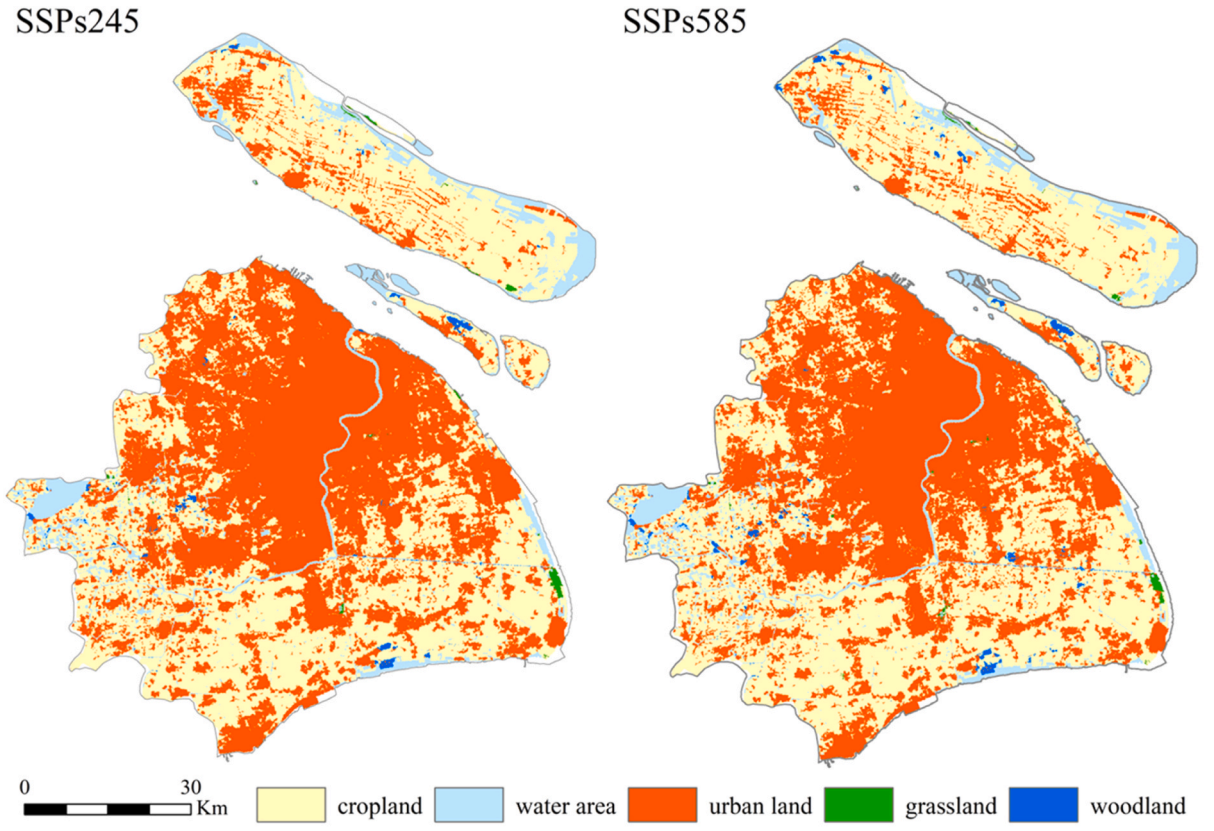

SSPs245 Type	Crop land	Water area	Urban land	Grass land	Wood land	SSPs585 Type	Crop land	Water area	Urban land	Grass land	Wood land
Area (km^2)	3040.92	481.85	3105.33	16.12	32.32	Area (km^2)	3260.55	481.85	2870.52	14.15	49.47

Fig. 9. Simulation of land use under SSPs245 and SSPs585 scenarios in 2100.

the SSPs585 scenario, urban development predominantly sprawls outward from the heart of Shanghai's city centre, while under the SSPs245 scenario, a more distinct development trajectory emerges in the Chongming island region.

Built-up land and agricultural land are the two major land use types in Shanghai. Built-up land is expected to grow by 24.30 %-34.47 % by 2100, While, agricultural land is expected to shrink the most with a decrease of 13.21 %-19.06 %. Natural land such as woodland and grassland, on the other hand, are projected to remain stable in relative amounts. These results suggest that future urban construction land in Shanghai may have a significant impact on agricultural land compared to natural land such as woodland and grassland. This trend is further supported by Fig. 9, which shows that agricultural land is expected to be significantly developed by 2100.

4.2. Impact of climate change on tropical cyclone floods

We use storm surge wave levels generated by simulated synthetic tropical cyclone events as boundary conditions, and combine spatially varying Manning coefficient to drive the SFINCS model for the simulation of storm surge flood hazards. In this analysis, the spatial distribution of Manning's n values was derived from the 2020 land cover map, and remained fixed for both SSPs245 and SSPs585 scenarios to isolate the influence of climate change from other factors. Fig. 10 shows the inundation maps of 1000-year TC storm surge floods under these two climate scenarios. The regions affected by storm surge flooding are usually characterized as dry, but they become wet during the 1000-year TC storm flood events. We observe that while the 1000-year TC is the main driver of storm surge floods, the influence of climate change driven factors results in distinct patterns of inundation extent and depth. Specifically, in the SSPs245 scenario, storm surge floods induced by a 1000-year TC inundate a small portion of the low-lying coastal floodplain in the northeast of Chongming Island. However, in the SSPs585 scenario, significant portions of Chongming Island and Changxing Island, particularly the coastal areas of Pudong District, are submerged by floods. Furthermore, we find that the impact of storm surge floods on the urban area of Shanghai appears relatively minor, potentially due to the combined effects of TC trajectories and the high

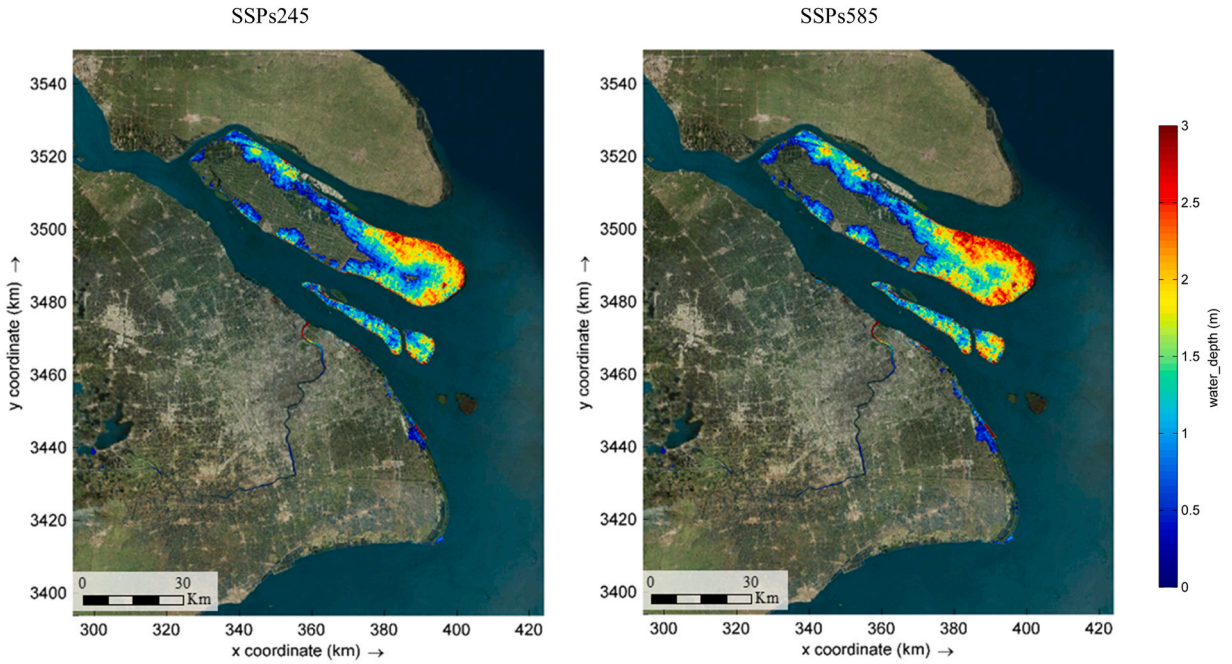

Fig. 10. Map of storm surge floods inundation for the 1000-year TC.

embankment protection standards in the urban area.

Furthermore, we conducted a statistical analysis of inundation depth and area, and categorized the inundation depth into four levels: shallow water (depth < 0.5 m), intermediate depth water (depth between 0.5 and 1 m), deep water (depth between 1 and 2 m), and extremely deep water (depth > 2 m). Table 3 shows the area and proportion of each inundation depth level. We found that the total flooded area increases by 135.37 km^2 under the SSPs585 compared to the SSPs245 scenario, and the proportion of inundated areas with deep water and above is the largest. Specifically, in the SSPs245 scenario, deep water inundation accounts for the highest proportion at 42.81 %, with extremely deep water inundation at 16.43 %. Similarly, in the SSPs585 scenario, deep water inundation still has the largest proportion at 43.31 %, and extremely deep water inundation accounts for 22.37 %. This indicates that Shanghai will still be affected by great storm surge flood in future.

4.3. The impact of land use change on flooding

Building on the analysis of climate-driven flood changes in Section 4.2, we further assess the additional impact of land use change on future flood inundation patterns by comparing current land use (CL) and projected future land use (FL) scenarios under the same climate forcings. The impact of land use on storm floods is assessed through the consideration of spatial changes in land use. Here, we compare the impact of land use change on storm flooding under current land use conditions and future climate scenarios, incorporating sea level rise into the future climate scenarios (Fig. 11). The prediction results reveal significant difference in storm flooding when future land use changes are considered or neglected. Specifically, the flood inundation areas indicated by current land use types are found to be lower than those projected under future land use scenarios (Table 4). Under the SSPs245 scenario, the maximum inundation area increases from 538.90 km^2 (CL245) to 553.15 km^2 (FL245), Under the SSPs585 scenario, the increase is more pronounced—from 524.67 km^2 (CL245) to 541.65 km^2 (FL245). In other words, ignoring future land use changes leads to an underestimation of the storm flood inundation areas. As urban land increases and natural areas decrease, surfaces with lower roughness become more dominant, resulting in a larger flood inundation extent under future scenarios. We also counted the maximum relative rate of change in the flood area, and found that ignoring land use changes would lead to an underestimation of the flood area by 4.91 % in the SSPs245 scenario (Fig. 11-b black error bar)., whereas this relative rate of change reaches 34.00 % in the SSPs585

Table 3
Statistics of flood depth.

Category	< 0.5 m		0.5–1 m		1–2 m		> 2 m		**Total** /km^2
	Area/ km^2	Ratio/%	Area/ km^2	Ratio/%	Area/ km^2	Ratio/%	Area/ km^2	Ratio/%	
SSPs245	186.13	18.61	221.56	22.15	428.20	42.81	164.37	16.43	1000.26
SSPs585	185.52	16.34	204.25	17.99	491.87	43.31	253.99	22.37	1135.63

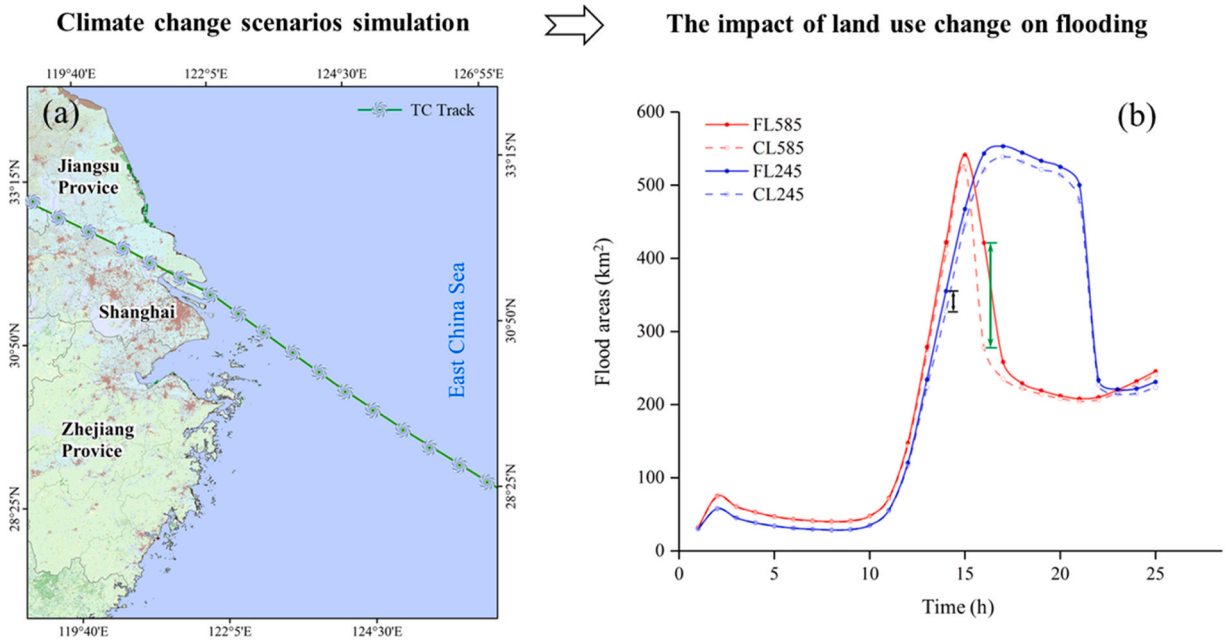

Fig. 11. Comparison of land use change impacts on flood inundation area. (FL585: future land use change and SSPs585 climate scenario; CL585: current conditions land use and SSPs585 climate scenario; FL245: future land use change and SSPs245 climate scenario; CL245: current conditions land use and SSPs245 climate scenario. The green error bars in Fig. A indicate the difference in the maximum flooded area at a certain moment under the same scenario).

Table 4
Statistics on the flood inundation area.

Scenario	CL245	FL245	CL585	FL585
Maximum flood inundation areas / km^2	538.90	553.15	524.67	541.65

scenario (Fig. 11-b green error bar). Furthermore, our results indicate that land use changes also affect the duration of flood events. Compared to the SSPs245 scenario, floods under the SSPs585 scenario recede faster. This is because, although the Chongming area experiences significant flood inundation in both scenarios, more built-up land types occur in the area at the same time under the SSPs245 scenario, which prolongs the flood recession time. This also suggests that Shanghai should control the expansion of built-up areas and preferably adopt nature-based solutions to reduce the adverse impacts of flood hazard in the future.

5. Discussion

5.1. Mechanisms of flood amplification under climate and land use change scenarios

The results of the study reveal that storm surge flood extent and depth increase markedly under the SSPs585 scenario compared to SSPs245. This amplification is driven by both climate-induced intensification of tropical cyclones and the projected expansion of urban impervious surfaces. Specifically, urban growth reduces surface roughness (Manning's n) and infiltration capacity, facilitating faster flow propagation and extended inundation duration (Deng et al., 2022). In particular, low-lying areas such as Chongming Island are increasingly exposed, as future land use scenarios predict significant conversion to built-up land, which accelerates overland water spread and reduces flood storage potential.

Although this study did not explicitly simulate infiltration due to the absence of TC rainfall scenarios, we recognize that infiltration into the subsurface layer is a critical factor influencing flood dynamics. In future studies, we plan to incorporate spatially varying infiltration rates based on land use and soil properties, which can be modeled through Curve Number (CN) methods or Manning's n adjustments. These refinements will allow future models to better capture infiltration processes and their interaction with land use changes and flood risks.

5.2. Comparison with existing studies and scientific implications

Our findings are consistent with previous studies emphasizing the importance of both climate change and land use dynamics in

shaping coastal flood risks. Neumann et al. (2015) highlighted that rapid urban expansion in low-elevation coastal zones, particularly in Asia, significantly increases population exposure to coastal flooding. Yin et al. (2021) emphasized the importance of climate change in shaping future coastal storm flood risks. In addition, Kulp and Strauss (2019) showed that urban expansion in low-lying deltas increases long-term storm surge exposure under sea level rise. Our findings further support this trend, particularly in Chongming Island, where projected impervious land use substantially elevates flood exposure.

Moreover, this study extends previous work by integrating high-resolution storm surge modeling (Delft3D and SFINCS) with dynamic land use projections (GeoSOS-FLUS). While earlier studies (e.g., Bilskie et al., 2022; Lai et al., 2020) emphasized climate forcing, they often assumed static land cover. By contrast, our approach reveals that neglecting future land use change can lead to flood extent underestimations of up to 34 %, highlighting urbanization as a critical but underappreciated driver of future hazard dynamics.

5.3. Limitations and future directions of this study

While the modeling framework improves our understanding of storm surge flood risk under compound climate and land use scenarios, some limitations remain. The current analysis does not incorporate fluvial or pluvial flooding, river discharges, or precipitation-induced infiltration, which may exacerbate compound flooding through surge–river interactions in estuarine environments. Additionally, the nesting scheme of Delft3D does not include feedback from wave forces to currents, which may influence surge propagation in complex coastal zones (Rego and Li, 2010). In addition, urban heat island effects and their potential to intensify tropical cyclone rainfall (Zhang et al., 2018) were also not considered but represent important directions for future research. These effects can amplify storm intensity and shift rainfall patterns, further increasing urban flood risk. Incorporating thermodynamic feedbacks, rainfall-runoff processes, and socio-economic vulnerability assessments would improve future flood impact modeling.

From a policy perspective, our results suggest that long-term urban planning in coastal megacities like Shanghai should account for both projected climate risks and land development pathways. Spatially explicit flood hazard maps under future land use scenarios can help guide zoning, infrastructure investment, and nature-based solutions, particularly in vulnerable regions such as Chongming and Changxing islands. Our framework is transferable to other coastal deltas, offering a scalable tool for climate-resilient urban planning worldwide.

6. Conclusions

We present a method for quantifying the impact of future coastal land use changes on storm surge flooding, integrating land use prediction models with storm surge hydrodynamic models. This study reveals several key findings and provides crucial insights for both scientific understanding and practical application:

(1) Urban Expansion Patterns and Flooding Risks: The study predicts that urban expansion in Shanghai will primarily occur outward from the city center, as well as into areas like Chongming island. This urban growth increases exposure to flood risks, particularly in low-lying coastal areas. These findings underscore the necessity of proactive urban planning that incorporates flood resilience into future city development.

(2) Impact of climate change and urbanization on storm surge flooding: The results demonstrate that future urban land use changes will lead to a significant increase in the extent of storm surge flooding, with a 4.91–34.00 % increase in flooded areas by 2100. This highlights the critical importance of considering urban land use changes in flood risk assessments and emphasizes the risk of underestimating flooding if future developments are not accounted for.

(3) The findings underscore the heightened vulnerability of coastal areas such as Chongming and Changxing islands to climate-driven storm surge hazards, even with existing embankment protections. This vulnerability is compounded by the effects of climate change, which will exacerbate the flooding risks in these regions. Therefore, there is an urgent need for enhanced flood mitigation measures and adaptive capacity improvements in these areas to better cope with future flood risks.

The results make an important contribution to a better understanding of how future urban land use changes will affect storm surge flooding hazards in the Shanghai, and improve our understanding of the extent to what extent incremental land use changes alter the reality of storm flood hazards. Future research should consider integrating rainfall and infiltration effects in hydrodynamic models to more accurately simulate the compound impacts of land use and climate change. Moreover, this framework is transferable to tropical cyclone-vulnerable coastal regions worldwide, providing a valuable tool for assessing and enhancing flood-mitigation strategies.

CRediT authorship contribution statement

Qinke Sun: Writing – review & editing, Writing – original draft, Validation, Software, Methodology, Investigation, Conceptualization. **Johan Reyns:** Writing – review & editing, Supervision, Resources, Methodology, Funding acquisition, Conceptualization. **Jiayi Fang:** Writing – review & editing, Validation, Methodology, Conceptualization. **Xiaoting Wang:** Writing – review & editing, Visualization, Software. **Zhe Wang:** Visualization, Resources, Methodology, Data curation. **Liang Zhou:** Writing – review & editing, Visualization, Validation, Resources. **Min Liu:** Writing – review & editing, Supervision, Funding acquisition, Conceptualization.

Declaration of Competing Interest

The authors declare that they have no known competing financial interests or personal relationships that could have appeared to influence the work reported in this paper.

Acknowledgments

This study was supported by the Youth Science and Technology Foundation of Gansu Province (No. 25JRRA209), Major Projects of Joint Scientific Research Fund of Gansu Province (No. 25JRRA1156), Joint Innovation Fund Project of Lanzhou Jiaotong University and Corresponding Supporting University (No. LH2025012), and the AXA Research Fund. The authors are grateful to Professor Roshanka Ranasinghe for his valuable suggestions. We would also like to thank the valuable suggestions and guidance provided by two anonymous reviewers.

Appendix A. Supporting information

Supplementary data associated with this article can be found in the online version at doi:10.1016/j.ejrh.2025.102745.

Data availability

Data will be made available on request.

References

Adnan, M.S.G., Abdullah, A.Y.M., Dewan, A., Hall, J.W., 2020. The effects of changing land use and flood hazard on poverty in coastal Bangladesh. Land Use Policy 99, 104868.
Amare, M.T., Demissie, S.T., Beza, S.A., Erena, S.H., 2024. Impacts of land Use/Land cover changes on the hydrology of the fafan catchment Ethiopia. J. Geovisualization Spat. Anal. 8 (1), 10.
Bastidas, L.A., Knighton, J., Kline, S.W., 2015. Parameter sensitivity and uncertainty analysis for a storm surge and wave model. Nat. Hazard. Earth Syst. Sci. Discuss. 3, 6491–6534.
Bates, P.D., Horritt, M.S., Fewtrell, T.J., 2010. A simple inertial formulation of the shallow water equations for efficient two-dimensional flood inundation modelling. J. Hydrol. 387 (1-2), 33–45.
Bhatia, K.T., Vecchi, G.A., Knutson, T.R., Murakami, H., Kossin, J., Dixon, K.W., Whitlock, C.E., 2019. Recent increases in tropical cyclone intensification rates. Nat. Commun. 10 (1), 635.
Bilskie, M.V., Angel, D.D., Yoskowitz, D., Hagen, S.C., 2022. Future flood risk exacerbated by the dynamic impacts of sea level rise along the Northern Gulf of Mexico. Earth's. Future 10 (4), e2021EF002414.
Bloemendaal, N., Haigh, I.D., de Moel, H., Muis, S., Haarsma, R.J., Aerts, J.C., 2020. Generation of a global synthetic tropical cyclone hazard dataset using STORM. Sci. Data 7 (1), 40.
Chen, Y., Li, X., Liu, X., Ai, B., 2014. Modeling urban land-use dynamics in a fast developing city using the modified logistic cellular automaton with a patch-based simulation strategy. Int. J. Geogr. Inf. Sci. 28 (2), 234–255.
Chu, D., Zhang, J., Wu, Y., Jiao, X., Qian, S., 2019. Sensitivities of modelling storm surge to bottom friction, wind drag coefficient, and meteorological product in the east China Sea. Estuar. Coast. Shelf Sci. 231, 106460.
Deltares, 2021. WES-Wind enhance scheme for cyclone modelling-User manual. Version.3. 01. SVN. Revision: 68491.
Deng, Z., Wang, Z., Wu, X., Lai, C., Zeng, Z., 2022. Strengthened tropical cyclones and higher flood risk under compound effect of climate change and urbanization across China's greater bay area. Urban Clim. 44, 101224.
Diakakis, M., Deligiannakis, G., Katsetsiadou, K., Lekkas, E., 2015. Hurricane sandy mortality in the Caribbean and continental North America. Disaster Prev. Manag. 24 (1), 132–148.
Du, J., Qian, L., Rui, H., Zuo, T., Zheng, D., Xu, Y., Xu, C.Y., 2012. Assessing the effects of urbanization on annual runoff and flood events using an integrated hydrological modeling system for qinhuai river basin, China. J. Hydrol. 464, 127–139.
Du, S., Scussolini, P., Ward, P.J., Zhang, M., Wen, J., Wang, L., Kok, E., Diaz-Loaiza, A., Gao, J., Ke, Q., Aerts, J.C., 2020. Hard or soft flood adaptation? Advantages of a hybrid strategy for shanghai. Glob. Environ. Change 61, 102037.
Dullaart, J.C., Muis, S., Bloemendaal, N., Chertova, M.V., Couasnon, A., Aerts, J.C., 2021. Accounting for tropical cyclones more than doubles the global population exposed to low-probability coastal flooding. Commun. Earth Environ. 2 (1), 135.
Fang, J., Lincke, D., Brown, S., Nicholls, R.J., Wolff, C., Merkens, J.L., Hinkel, J., Vafeidis, A., Shi, P., Liu, M., 2020. Coastal flood risks in China through the 21st century–An application of DIVA. Sci. Total Environ. 704, 135311.
Gori, A., Blessing, R., Juan, A., Brody, S., Bedient, P., 2019. Characterizing urbanization impacts on floodplain through integrated land use, hydrologic, and hydraulic modeling. J. Hydrol. 568, 82–95.
Gori, A., Lin, N., Xi, D., Emanuel, K., 2022. Tropical cyclone climatology change greatly exacerbates US extreme rainfall–surge hazard. Nat. Clim. Change 12 (2), 171–178.
Guzha, A.C., Rufino, M.C., Okoth, S., Jacobs, S., Nóbrega, R.L.B., 2018. Impacts of land use and land cover change on surface runoff, discharge and low flows: evidence from east Africa. J. Hydrol. Reg. Stud. 15, 49–67.
Hallegatte, S., Green, C., Nicholls, R.J., Corfee-Morlot, J., 2013. Future flood losses in major coastal cities. Nat. Clim. Change 3 (9), 802–806.
Hanson, S., Nicholls, R., Ranger, N., Hallegatte, S., Corfee-Morlot, J., Herweijer, C., Chateau, J., 2011. A global ranking of port cities with high exposure to climate extremes. Clim. Change 104, 89–111.
Hinkel, J., Aerts, J.C., Brown, S., Jiménez, J.A., Lincke, D., Nicholls, R.J., Scussolini, P., Sanchez-Arcilla, A., Vafeidis, A., Addo, K.A., 2018. The ability of societies to adapt to twenty-first-century sea-level rise. Nat. Clim. Change 8 (7), 570–578.
Holland, G.J., Belanger, J.I., Fritz, A., 2010. A revised model for radial profiles of hurricane winds. Mon. Weather Rev. 138 (12), 4393–4401.
Hou, H., Zhou, B.B., Pei, F., Hu, G., Su, Z., Zeng, Y., Zhang, H., Gao, Y., Luo, M., Li, X., 2022. Future land use/land cover change has nontrivial and potentially dominant impact on global gross primary productivity. Earth's. Future 10 (9), e2021EF002628.
Jongman, B., Hochrainer-Stigler, S., Feyen, L., Aerts, J.C., Mechler, R., Botzen, W.W., Bouwer, L., Pflug, G., Rojas, R., Ward, P.J., 2014. Increasing stress on disaster-risk finance due to large floods. Nat. Clim. Change 4 (4), 264–268.
Kalyanapu, A.J., Burian, S.J., McPherson, T.N., 2009. Effect of land use-based surface roughness on hydrologic model output. J. Spat. Hydrol. 9 (2), 51–71.
Knutson, T.R., McBride, J.L., Chan, J., Emanuel, K., Holland, G., Landsea, C., Held, I., Kossin, J.P., Srivastava, A.K., Sugi, M., 2010. Tropical cyclones and climate change. Nat. Geosci. 3, 157–163.
Koks, E.E., Rozenberg, J., Zorn, C., Tariverdi, M., Vousdoukas, M., Fraser, S.A., Hall, J.W., Hallegatte, S., 2019. A global multi-hazard risk analysis of road and railway infrastructure assets. Nat. Commun. 10 (1), 2677.
Kulp, S.A., Strauss, B.H., 2019. New elevation data triple estimates of global vulnerability to sea-level rise and coastal flooding. Nat. Commun. 10 (1), 1–12.

Lai, Y., Li, J., Gu, X., Chen, Y., Kong, D., Gan, T.Y., Liu, M., Li, Q., Wu, G., 2020. Greater flood risks in response to slowdown of tropical cyclones over the coast of China. Proc. Natl. Acad. Sci. 117 (26), 14751–14755.
Leijnse, T., van Ormondt, M., Nederhoff, K., van Dongeren, A., 2021. Modeling compound flooding in coastal systems using a computationally efficient reduced-physics solver: including fluvial, pluvial, tidal, wind-and wave-driven processes. Coast. Eng. 163, 103796.
Lesser, G.R., Roelvink, J.V., van Kester, J.T.M., Stelling, G.S., 2004. Development and validation of a three-dimensional morphological model. Coast. Eng. 51 (8-9), 883–915.
Li, X., Yeh, A.G.O., 2002. Neural-network-based cellular automata for simulating multiple land use changes using GIS. Int. J. Geogr. Inf. Sci. 16 (4), 323–343.
Li, X., Chen, Y., Liu, X., Li, D., He, J., 2011. Concepts, methodologies, and tools of an integrated geographical simulation and optimization system (GeoSOS). Int. J. Geogr. Inf. Sci. 25 (4), 633–655.
Liu, J., Xiong, J., Chen, Y., Sun, H., Zhao, X., Tu, F., Gu, Y., 2023. An integrated model chain for future flood risk prediction under land-use changes. J. Environ. Manag. 342, 118125.
Liu, X., Liang, X., Li, X., Xu, X., Ou, J., Chen, Y., Li, S., Wang, S., Pei, F., 2017. A future land use simulation model (FLUS) for simulating multiple land use scenarios by coupling human and natural effects. Landsc. Urban Plan. 168, 94–116.
Lu, X., Yu, H., Ying, M., Zhao, B., Zhang, S., Lin, L., Bai, L., Wan, R., 2021. Western north pacific tropical cyclone database created by the China meteorological administration. Adv. Atmos. Sci. 38, 690–699.
Lyddon, C.E., Brown, J.M., Leonardi, N., Saulter, A., Plater, A.J., 2019. Quantification of the uncertainty in coastal storm hazard predictions due to wave-current interaction and wind forcing. Geophys. Res. Lett. 46 (24), 14576–14585.
Mazumder, A., Sarkar, A., Sikder, M.B., Tabassum, A., Islam, S.T., Barua, E., 2024. Impact of land conversion on land surface temperature over the coastal area: a spatiotemporal study of Cox's bazar district, Bangladesh. J. Geovisualization Spat. Anal. 8 (2), 35.
Neumann, B., Vafeidis, A.T., Zimmermann, J., Nicholls, R.J., 2015. Future coastal population growth and exposure to sea-level rise and coastal flooding-a global assessment. PloS One 10 (3), e0118571.
Orton, P.M., Conticello, F.R., Cioffi, F., Hall, T.M., Georgas, N., Lall, U., Blumberg, A.F., MacManus, K., 2018. Flood hazard assessment from storm tides, rain and sea level rise for a tidal river estuary. Nat. Hazards 102 (2), 729–757.
Pan, Z.H., Liu, H., 2019. Extreme storm surge induced coastal inundation in Yangtze estuary regions. J. Hydrodyn. 31 (6), 1127–1138.
Pumo, D., Arnone, E., Francipane, A., Caracciolo, D., Noto, L.V., 2017. Potential implications of climate change and urbanization on watershed hydrology. J. Hydrol. 554, 80–99.
Qiang, Y., Lam, N.S., 2015. Modeling land use and land cover changes in a vulnerable coastal region using artificial neural networks and cellular automata. Environ. Monit. Assess. 187, 1–16.
Ranasinghe, R., Duong, T.M., Uhlenbrook, S., Roelvink, D., Stive, M., 2013. Climate-change impact assessment for inlet-interrupted coastlines. Nat. Clim. Change 3 (1), 83–87.
Rego, J.L., Li, C., 2010. Nonlinear terms in storm surge predictions: effect of tide and shelf geometry with case study from hurricane rita. J. Geophys. Res. 115, C005285.
Sajikumar, N., Remya, R.S., 2015. Impact of land cover and land use change on runoff characteristics. J. Environ. Manag. 161, 460–468.
Schilling, K.E., Chan, K.S., Liu, H., Zhang, Y.K., 2010. Quantifying the effect of land use land cover change on increasing discharge in the upper Mississippi River. J. Hydrol. 387 (3-4), 343–345.
Sebastian, A., 2022. Compound flooding. In Coastal Flood Risk Reduction. Elsevier, pp. 77–88.
Shao, M., Zhao, G., Kao, S.C., Cuo, L., Rankin, C., Gao, H., 2020. Quantifying the effects of urbanization on floods in a changing environment to promote water security—A case study of two adjacent basins in texas. J. Hydrol. 589, 125154.
Sun, Q., Fang, J., Dang, X., Xu, K., Fang, Y., Li, X., Liu, M., 2022. Multi-scenario urban flood risk assessment by integrating future land use change models and hydrodynamic models. Nat. Hazards Earth Syst. Sci. 22 (11), 3815–3829.
Townsend, Frances Fragos, 2006. Fed. Response Hurric. Katrina Lessons Learn.
Verburg, P.H., Soepboer, W., Veldkamp, A., Limpiada, R., Espaldon, V., Mastura, S.S., 2002. Modeling the spatial dynamics of regional land use: the CLUE-S model. Environ. Manag. 30, 391–405.
Vousdoukas, M.I., Mentaschi, L., Voukouvalas, E., Verlaan, M., Jevrejeva, S., Jackson, L.P., Feyen, L., 2018. Global probabilistic projections of extreme sea levels show intensification of coastal flood hazard. Nat. Commun. 9 (1), 2360.
Wang, J., Yi, S., Li, M., Wang, L., Song, C., 2018. Effects of sea level rise, land subsidence, bathymetric change and typhoon tracks on storm flooding in the coastal areas of shanghai. Sci. Total Environ. 621, 228–234.
Wu, S., Zhou, X., Reyns, J., Yamazaki, D., Yin, J., Li, X., 2024. Climate change and urban sprawl: unveiling the escalating flood risks in river deltas with a deep dive into the GBM river delta. Sci. Total Environ. 947, 174703.
Xu, H., Li, X., 2019. Sensitivity of WRF model simulations to parametrizations of depositional growth of ice crystal during the landfall of typhoon fitow (2013). Q. J. R. Meteorol. Soc. 145 (722), 2161–2180.
Xu, X., Liu, J., Zhang, S., Li, R., Yan, C., Wu., S., 2018. China's Multi-Period Land Use Land Cover Remote Sensing Monitoring Data Set (CNLUCC). Resour. Environ. Data Cloud Platf. ⟨http://www.resdc.cn/DOI⟩.
Yin, J., 2020. Simul. flooding embankment breaches Delft3D Flex. Mesh Case Study Coast. Area Shanghai TU Delft.
Yin, J., Lin, N., Yang, Y., Pringle, W.J., Tan, J., Westerink, J.J., Yu, D., 2021. Hazard assessment for typhoon-induced coastal flooding and inundation in shanghai, China. J. Geophys. Res. Oceans 126 (7) e2021JC017319.
Zhang, W., Villarini, G., Vecchi, G.A., Smith, J.A., 2018. Urbanization exacerbated the rainfall and flooding caused by hurricane harvey in houston. Nature 563 (7731), 384–388.
Zong, Y., Chen, X., 2002. Typhoon hazards in the shanghai area. Disasters 23 (1), 66–80.